# Photocurrent Spectroscopy of (*n*, *m*) Sorted Solution-Processed Single-Walled Carbon Nanotubes

**Michael Engel,[†,#] Katherine E. Moore,[†,‡] Asiful Alam,[†] Simone Dehm,[†] Ralph Krupke,[†,§,*] and Benjamin S. Flavel[†,*]**

[†]Institute of Nanotechnology, Karlsruhe Institute of Technology, 76021, Karlsruhe, Germany, [‡]Centre for Nanoscale Science and Technology, School of Chemical and Physical Sciences, Flinders University, 5000, Adelaide, Australia, and [§]Institute for Materials Science, Technische Universität Darmstadt, 64287, Darmstadt, Germany. [#]Present address: IBM Thomas J. Watson Research Center, Yorktown Heights, New York 10598, United States.

**ABSTRACT** Variable-wavelength photocurrent microscopy and photocurrent spectroscopy are used to study the photoresponse of (*n*, *m*) sorted single-walled carbon nanotube (SWNT) devices. The measurements of (*n*, *m*) pure SWCNT devices demonstrate the ability to study the wavelength-dependent photoresponse *in situ* in a device configuration and deliver photocurrent spectra that reflect the population of the source material. Furthermore, we show that it is possible to map and determine the chirality population within a working optoelectronic SWCNT device.

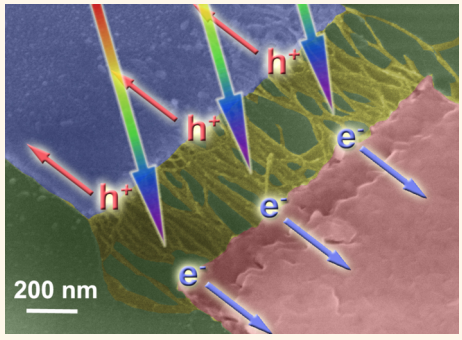


**KEYWORDS:** spectrally resolved photocurrent · carbon nanotube · chirality sorted · supercontinuum light source

Recently the use of single-walled carbon nanotubes (SWCNTs) for next-generation all-carbon solar cells and light-sensitive devices has gained increasing attention in the literature.[1] While SWCNTs have traditionally been integrated into a variety of organic photovoltaic systems, the role of carbon nanotubes in these systems was strictly limited to their use as an efficient electron transport medium. The latest focus is aimed at capitalizing on the unique and richly varying optical properties of SWCNTs. In order to appreciate this point, it is only necessary to consider the SWCNTs produced by the HiPco process and the possible applications they may have for photovoltaics. The HiPco raw material consists of a multitude of semiconducting (s-SWCNT) species of varying diameter ($D_t$), chiral angle, or (*n*, *m*) index, and each of these species has unique first ($S_{11}$) and second ($S_{22}$) optical transitions in the region ~900−1350 nm and ~500−850 nm, respectively.[2,3] Therefore, upon selecting the appropriate (*n*, *m*) combination of SWCNTs, it is theoretically possible to fabricate a solar cell capable of harvesting light in not only the visible but also the infrared,[4] a spectral region excluded by traditional silicon solar cells. Alternatively, it is envisaged that upon selecting highly pure (*n*, *m*) material, it would be possible to create a device that is sensitive to the discrete optical transitions of the SWCNTs, hence paving the way for optical sensors.[5] This discussion can then of course be extended to consider other SWCNT synthetic routes such as arc discharge, laser ablation, and the CoMoCAT process, which afford a completely different ensemble of (*n*, *m*) species and extend the accessible spectral regime, not to mention the possibility of probing higher order optical transitions ($S_{33}$, $S_{44}$, *etc.*), multiple exciton generation,[6] and the potential for metallic SWCNTs (m-SWCNTs) to be used as metallic contacts.

The realization of these goals has led to the development of several different approaches. Toward the fabrication of solar cells from thin films of SWCNTs, Svreck *et al.*[7] have combined poly-9,9-di-*n*-octylfluorenyl-2,7-diyl (PFO)-wrapped SWCNTs with silicon nanocrystals and shown that the photocurrent is unambiguously correlated to the optical properties of the nanotubes. Likewise, Bindl *et al.*[8,9] integrated PFO-wrapped SWCNTs

* Address correspondence to benjamin.flavel@kit.edu, ralph.krupke@kit.edu.

Received for review June 17, 2014 and accepted August 12, 2014.

**Published online August 12, 2014**
**10.1021/nn503278d**

into bilayered heterojunctions with $C_{60}$ as an acceptor. Jain *et al.*[10] then demonstrated the viability of this bilayered heterojunction approach with polymer-unwrapped, surfactant-stabilized, (6,5) SWCNTs. Despite initial SWCNT/$C_{60}$ solar cells boasting relatively low efficiencies, Shea *et al.*[11] have recently reported efficiencies of up to 1%. Nevertheless, it remains clear that further work is required in order to achieve devices comparable to other well-established organic photovoltaic systems. Perhaps this is indeed achieved through using multiple nanotube layers as suggested by Shea *et al.*,[11] but the field also benefits from photocurrent studies on the single- or few-nanotube level, where a more fundamental investigation of the generation of photocurrent is possible.

From a technological standpoint the fabrication of single- or few-nanotube devices is not new. Techniques such as dielectrophoretic deposition from solution[12,13] or chemical vapor deposition (CVD) growth of SWCNTs between metalized source and drain contacts in CNT field-effect transistors are becoming standard. In this architecture photogenerated electrons and holes are typically separated by either an externally applied gate bias or internal fields at the SWCNT−metal Schottky barrier.[14,15,39,40] Photocurrent generation has therefore been studied in both substrate-supported[6,16−19] and unsupported[20−22] CNTs. However, unlike in the case of the SWCNT films discussed previously, a laser is typically used to address the CNTs due to the high power density required to measure photocurrent from only a few CNTs. Hence the laser source and CNT must be chosen carefully to ensure at least one of the CNT's optical transitions (usually $S_{22}$) matches the excitation source. From this point of view one could call such systems "nanoscale solar cells"; however, as the ability to produce power under illumination on the single-nanotube level is yet to be shown, it is more realistic to refer to them as "nanoscale photodetectors" or simply appreciate the fundamental spectroscopic investigation that is possible on this scale. The literature contains many such examples. For example the early work of Chen *et al.*[16] and further work by Engel *et al.*[17] using SWCNTs placed between asymmetric metal contacts (with high and low work function) to achieve a strong built-in electric field allowed for the efficient separation of electron−hole pairs. Alternatively, Lee *et al.*[19,22] formed a p−n junction along the length of a single carbon nanotube by electrostatic doping using a pair of split gate electrodes. Electron−hole pairs were then separated in the middle of the device where the electric field was the greatest.

Most recently, Barkelid *et al.*[20,21] used a similar split gate design and provided a comparison of the photocurrent generated in semiconducting and metallic carbon nanotubes. In their work they suggest that the photocurrent generated from semiconducting nanotubes had photovoltaic origins, whereas in the case of metallic nanotubes it was photothermoelectric. In other words the photocurrent in s-SWCNTs arises from an electric field (built-in or applied), and the photocurrent in m-SWCNTs is mediated by a difference in Seebeck coefficients. In performing their study Barkelid *et al.*[20,21] addressed a problem in the literature, namely, seemingly conflicting results with some reports stating the photocurrent to be photothermoelectric[23−26] in origin while others showed a photovoltaic behavior.[16,17,22] Reflecting on the device design of many groups reporting photothermoelectric origins, either unsorted metallic CNTs[24] or a film of CNTs was used.[23,27] Hence discrimination between these two effects was understandably difficult. However, in the work of Amer *et al.*,[28] who exclusively worked on split gate devices from metallic CNTs, it is important to note that the photocurrent signal was clearly seen to originate from the center of the nanotube (position of split gates), which would suggest that the photocurrent originated from the p−n junction rather than the contacts. Moreover, in 2014, DeBorde *et al.*[29] found evidence of both photovoltaic and photothermoelectric mechanisms, where the type of mechanism responsible was found to depend on the gate voltage, *i.e.*, if the carbon nanotube was in the off- or on-state, respectively. Indeed the discussion of photocurrent generation in CNTs appears to be far from resolved. More important at this point is the conclusion that if such fundamental studies are to be performed, the suspension of CNTs used, or growth mechanism applied, must be limited to CNTs of well-defined and controlled electronic and optical property.

Toward this end DeBorde *et al.*[30] have used chemical vapor deposition to integrate single-chirality carbon nanotubes into field-effect transistor devices. In their work, due to each device consisting of only one CNT, each device was by definition single chirality and correspondingly had well-defined optical properties. This allowed DeBorde *et al.*[30] to measure photoconductivity spectra for each device and identify the chiral indices upon comparison to a catalogue of known CNT exciton resonances. Consequently the use of photocurrent measurements may prove to be a useful characterization technique for device-integrated CNTs. Such a characterization tool would also be advantageous compared to traditional techniques involving the scattering of polarized light by CNTs,[31] where the point of measurement must be sufficiently far away from any metal contact to avoid Rayleigh scattering from the electrodes, therefore limiting the technique to long channel devices with long CNTs (~20 $\mu$m[31]). Although long channel devices are easily achieved with CVD growth, solution-processed CNTs typically have lengths on the order of a few micrometers and make such devices impractical. This is where photocurrent characterization may play an important role.

The use of solution-processed CNTs has the added advantage of being able to prepare single-chirality suspensions and thus prepare CNT devices with

predetermined (*n*, *m*) indices. This is different from CVD growth, where the type of CNT grown is unknown and varies between devices. For this reason many groups focus their efforts on solution processing of (*n*, *m*) pure SWCNTs. This has been achieved *via* techniques such as the wrapping of SWCNTs with single-stranded DNA (ssDNA),[32] density gradient ultracentrifugation,[33−35] and Sephacryl gel filtration.[36−38] In our contribution to this field we have recently shown that 15 different (*n*, *m*) semiconducting species can be prepared from the HiPco raw material using the Sephacryl gel filtration method upon changing the pH of the eluent.[2] Most recently we have then applied our technique to an automated gel permeation chromatography (GPC) system. This system is capable of applying controlled pH gradients to a gel column and allowed us to demonstrate the scalable preparation of semiconducting (*n*, *m*) species with a purity of 61−95%.[3] In the present work we now integrate the prepared (*n*, *m*) SWCNT species into two terminal electronic devices to allow the measurement of spectrally resolved photocurrent. Furthermore, to our knowledge this is the first example of photocurrent spectroscopy being used to characterize solution-processed SWCNTs.

## RESULTS AND DISCUSSION

With the use of dielectrophoresis, single-chirality SWCNTs were deposited into devices for the measurement of photocurrent. Each device consisted of two palladium contacts with a width of 1 $\mu$m and a gap-size (channel width) of 600 nm on a $Si/SiO_2$ substrate. To any set of palladium contacts either the (6, 5), (7, 6), (7, 5), (8, 3), or (9, 4) SWCNT species were deposited to yield a single-chirality SWCNT device. For each of the SWCNT species a corresponding solution absorption measurement is shown in Figure 1. As our measurement setup is currently capable of measurement only in the visible regime, only the $S_{22}$ region for each (*n*, *m*) species is shown. Complete spectra from 500−1300 nm for each (*n*, *m*) species, where both $S_{22}$ and $S_{11}$ are visible, along with the normalization factors used are available in Figure S1 of the Supporting Information. As expected for pure (*n*, *m*) SWCNT suspensions, every species has only one major $S_{22}$ resonance with no or minor additional resonances. We attribute minor resonances to the impurity of additional (*n*, *m*) SWNT species. This issue of impurities will be revisited later. Moreover, with the exception of (7, 5) and (7, 6), it can also be seen that all $S_{22}$ optical resonances are well separated. The position of each transition is further listed in Table 1. Each chirality therefore possesses a "fingerprint" that should be possible to resolve in a photocurrent spectroscopy experiment.

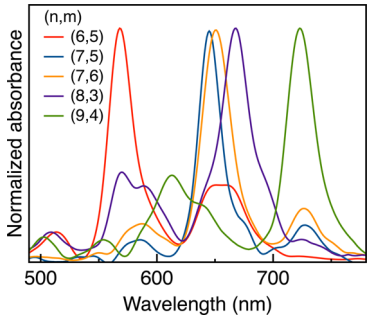


**Figure 1. Solution absorption spectra of the five different (*n*, *m*) SWNT species used in this work: (6, 5), (7, 5), (7, 6), (8, 3), and (9, 4).**

A typical device can be seen both schematically (a) and *via* SEM (b) in Figure 2, where in this case (6, 5) SWCNTs have been deposited between the contacts. It can also be clearly seen that the SWCNTs are predominantly aligned in the direction of the electric field during deposition and that they directly bridge the 600 nm gap. Consequently, the SWCNTs used in this work do not form a percolative current path. Instead each CNT individually contributes to the overall photocurrent measured. On average approximately 10−20 SWCNTs were deposited after dielectrophoresis.

Single-chirality devices were then placed into our custom-built setup for the measurement of photocurrent. In this setup the excitation source was a commercial supercontinuum light source with an attached acousto-optical tunable filter (AOTF) to provide the required wavelength selectivity. The light output was then fiber coupled into a microscope and focused onto the SWCNT device with an objective as seen in Figure 2a. Additionally the entire setup was placed onto an *x*−*y* piezoelectric table, which allowed for not only spectrally resolved photocurrent measurements but also 2D surface mapping.

A 2D photocurrent map is shown in Figure 2c, where the short-circuit photocurrent has been overlaid onto

**TABLE 1. Responsivity of Each (*n*, *m*) SWCNT Device and a Comparison of the $S_{22}$ Optical Transition Obtained from Solution Absorption and Photocurrent Spectroscopy**

| SWCNT (*n*, *m*) | super continuum light source power (mW) | peak photocurrent (pA) | responsivity (pA/mW) | photocurrent maxima (nm) | photocurrent fwhm (nm) | absorption maxima (nm) | absorption fwhm (nm) |
|---|---|---|---|---|---|---|---|
| (6, 5) | 0.24 | 52.00 | 216.67 | 557 | 47.7 | 569 | 23.8 |
| (7, 5) | 0.66 | 28.60 | 43.33 | 648 | 48.8 | 645 | 21.1 |
| (7, 6) | 0.66 | 31.00 | 46.97 | 644 | 46.1 | 651 | 26.8 |
| (8, 3) | 0.94 | 8.53 | 9.07 | 666 | 59.8 | 667 | 35.7 |
| (9, 4) | 2.38 | 6.28 | 2.64 | 706 | 52.9 | 723 | 27.1 |

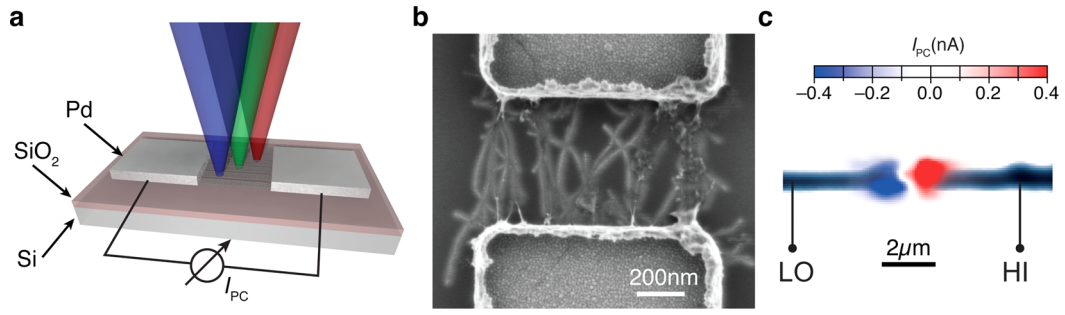


**Figure 2. (a) 3D schematic of the measurement setup. A focused light beam of variable wavelength is scanned across a carbon nanotube film interfaced with metallic contacts. (b) Scanning electron micrograph of a typical carbon nanotube device as schematically shown in (a), where the nanotube density is approximately 10/$\mu$m. (c) Scanning photocurrent microscopy map (excited at 570 nm) overlaid on top of the simultaneously recorded elastically scattered signal from the sample.**

the corresponding 2D map of elastically scattered light. In this example a device with (6, 5) SWCNT species was excited at 570 nm, corresponding to the $S_{22}$ optical transition for the (6, 5) SWCNT. As a comparison we also measure at off-resonant wavelengths and consistently observe a drop in the maximum photocurrent amplitude. The two metal contacts can clearly be seen on either side of the 2D map with two photocurrent lobes (blue minima and red maxima) located in the middle of the device. Hence we are able to spatially correlate the photocurrent with respect to the metallic contacts. It is noted that the photocurrent lobes are located close to the SWCNT−metal contact. This is to be expected due to the built-in electric field at the SWCNT−metal Schottky barrier being responsible for electron−hole separation. The presence of positive and negative photocurrent maxima is due to the use of symmetric palladium contacts. Therefore, the band bending due to dissimilar work functions of the metal and SWCNT are symmetric on either end of the SWCNT. Intuitively, when both SWCNT−metal contacts are equally illuminated by the light source (in the center of the device), an equal and opposite photocurrent will therefore be observed on either side of the SWCNT. This would consequently lead to a vanishing net overall photocurrent, a feature that is seen in the middle of our device in the 2D photocurrent map. The two photocurrent lobes therefore correspond to off-center excitation of the SWCNTs, where the photocurrent contribution from one end of the SWCNT outweighs that of the other end. In this work it is the translation of the light source across the device that ensures that such off-center excitation occurs.

For reference, representative transconductance curves for SWCNT devices can be found in Figure S2 of the Supporting Information. It can be seen that we observe p-type transfer characteristics for our devices. Upon noting which of the two palladium electrodes is placed on the high or low connection to the source meter, it is possible to determine the flow direction of carriers across the nanotube channel. In the setup the source meter is measuring the flow direction of electrons and not the technical current. From this standpoint we were able to determine that excitation of an SWCNT in our device through the $S_{22}$ transition leads to a flow of holes onto the palladium contact. This observation is then in agreement with the hole conductance seen in Figure S2.

With the ability to measure photocurrent from single-chirality nanotube devices we are therefore able to perform the main objective of this work, namely, the measurement of spectrally resolved photocurrent, where we would like to show a one-to-one correlation between optical absorption data and photocurrent. For these measurements the device was positioned under the beam *via* the $x-y$ table so as to maximize the photocurrent signal (*i.e.*, off-center photoexcitation of the device to maximize one of the photocurrent lobes). The sample position was then fixed and the wavelength swept between 500 and 750 nm in 5 nm steps. The reason for this is the finite spectral resolution of the AOTF, which outputs a single wavelength with a full-width at half-maximum (fwhm) of 5 nm. For each wavelength step we let the beam and photocurrent settle for three seconds. This proved to be a good compromise between signal-to-noise ratio and measurement speed with regard to position stability of the device.

In Figure 3 the photocurrent for the five different ($n$, $m$) SWNT devices can then be seen as a function of excitation wavelength. For each SWCNT species a clear peak in the photocurrent can be seen. This is attributed once again to electron−hole pairs formed through $S_{22}$ irradiation that get separated and subsequently collected at the contact. With the use of a calibrated silicon diode we then calculate the responsivity of each device, as can be found in Table 1. Furthermore, we make a comparison between the photocurrent peak position and that of the absorption measurement in solution. In general, good agreement between the peak position in the photocurrent and absorption data is seen. However, we do note that a slight blue-shift is seen for (7,5), (7,6), and (8,3) of 1−7 nm and a larger blue-shift for (6, 5) and (9, 4) of 12−17 nm. The exact

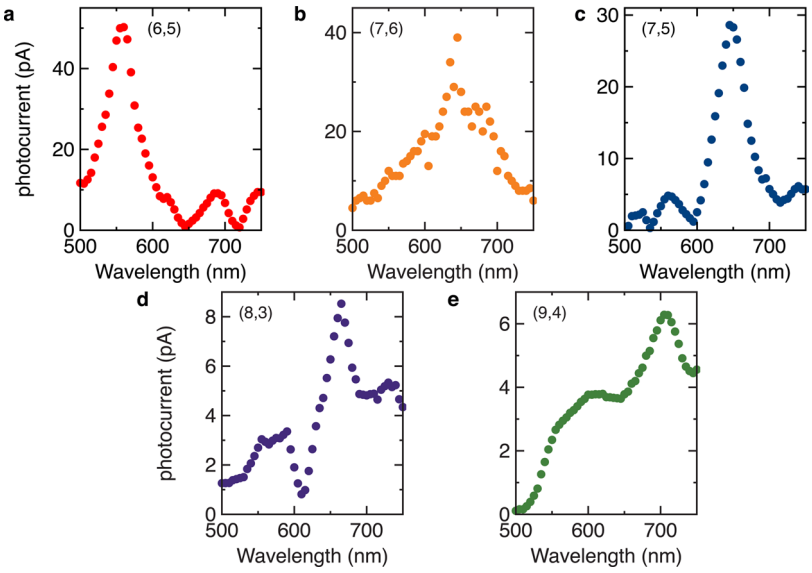


**Figure 3. Normalized photocurrent as a function of wavelength for carbon nanotube devices comprising (a) (6, 5), (b) (7, 5), (c) (7, 6), (d) (8, 3), and (e) (9, 4) SWNT species.**

origin of the observed blue-shift seen in our work remains speculative. As outlined in the Supporting Information from Liu *et al.*[31] it is well known that the optical resonances of carbon nanotubes are highly sensitive to the surrounding dielectric environment.[41−43] For example, the optical resonances of SWCNTs in micelle suspensions (as in our case for the absorption measurement) are typically red-shifted by 16 meV ($S_{22}$) and 28 meV ($S_{11}$) compared to free-suspended SWCNTs.[42] Likewise, Liu *et al.*[31] showed a 30 meV red-shift for SWCNTs on a $Si/SiO_2$ surface (the substrate used in our work) compared to free suspended SWCNTs. Furthermore, Fantini *et al.*[44] showed that bundling of carbon nanotubes leads to on average a 70 meV red-shift compared to suspended micelle-wrapped nanotubes. In our case the final dielectric environment for the SWCNTs in a device is complicated by the presence of different regions along the nanotube, all of which likely contribute to the final peak position that we see in the photocurrent. In our device we have a region of nanotube in contact with metal, a small region of free suspended nanotube (from the top of the metal contact to the substrate), and a region that is in contact with the silicon substrate. Additionally, there is the possibility for residual surfactants to be present and the formation of carbon nanotube bundles on the surface. All of these factors will give rise to a different dielectric environment for the nanotube, and how that will impact the peak position in photocurrent measurements remains unclear. Indeed we expected a red-shift as in the work of Liu *et al.*;[31] however other than to speculate that the observed blue-shift may be a result of the small free suspended region of nanotubes in close proximity to the metallic contact, this issue currently remains unclear to us. However, it can be seen

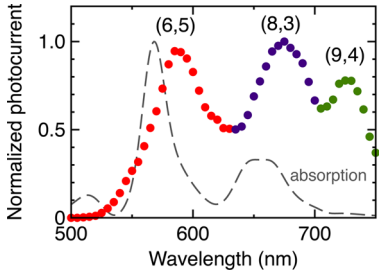


**Figure 4. Normalized photocurrent as a function of wavelength for a "high-density" carbon nanotube device. The photocurrent peaks are chirality assigned based on the absorption spectrum (gray).**

that the population of (*n*, *m*) SWNT species in solution is reflected in a device configuration.

The question now arises of whether photocurrent measurements can be used as a routine technique for the determination of (*n*, *m*) species in solution or on a surface. In this case the issue of impurity levels becomes important. This is an issue that is best addressed from a larger ensemble of SWCNTs so as to better replicate the entire population of SWCNTs. Due to the obvious presence of additional (*n*, *m*) species, the (6, 5) suspension used in this work was chosen as the ideal test solution. Once again dielectrophoresis was used to deposit the suspension; however an increased alternating voltage was used so as to afford a 10-fold increase in the number SWCNTs in the device. Figure 4 shows a plot of the measured photocurrent spectrum of such a device. As expected, instead of a single photocurrent peak at approximately 557 nm as in Figure 3, multiple photocurrent peaks became visible at 650 and 730 nm. Unexpected is the relative intensity of the additional photocurrent peaks. For comparison, the solution absorption spectrum of the (6, 5) SWCNT suspension is shown. Initially obvious is a red-shift of

the photocurrent peak, which as previously discussed is to be expected for a device containing a film of carbon nanotubes where bundling becomes a likely result. Additionally, minor peaks at 650 and 730 nm can also be seen in the absorption spectrum, but their intensity is significantly lower compared to the $S_{22}$ transition of (6, 5) at 557 nm. Here we attribute these peaks to (8, 3), (7, 5), or (9, 4) impurities. Benedict *et al.*[45] and Kozinsky *et al.*[46] help to provide an explanation of this result, by showing that the polarizability of semiconducting carbon nanotubes scales inversely proportional to the band gap. Therefore, nanotubes with a smaller band gap (larger diameter) are more easily deposited by dielectrophoresis. Here we argue that under the present assembly conditions that the larger diameter species such as (9, 4) and (7, 5) are deposited in preference to the smaller diameter (6, 5) SWCNT. This is despite the total contribution of (9, 4), (7, 5), and (8, 3) to the overall SWCNT population in solution being lower. From this point of view, SWCNT photocurrent measurements appear to be capable of providing qualitative information about a nanotube suspension, but their use in a quantitative analysis may be limited. Additionally, for any routine analysis of SWCNTs, the ability to probe not only $S_{22}$ but also $S_{11}$ optical transitions is necessary. This point is made especially clear upon examining the absorption data for the (7, 5), (7, 6), and (8, 3) SWCNTs. All of these species have an $S_{22}$ transition within the region of 640−660 nm (Figure 1). Consequently, upon consideration of only $S_{22}$, it would be difficult to determine the (*n*, *m*) species from truly unknown SWCNT suspensions. It is only in combination with the complementary $S_{11}$ data (Figure S1) that one obtains a reliable "fingerprint" for each (*n*, *m*) species. For this reason we plan to extend our measurement system with an additional AOTF capable of infrared selectivity.

## SUMMARY

In this work we have demonstrated photocurrent spectroscopy of single-chirality carbon nanotube optoelectronic devices and found that our results show good correlation with optical spectroscopy techniques. This technique may offer an *in situ* analytic tool for the characterization of future carbon nanotube devices. Alternatively, the ability to measure single-chirality photocurrent spectra paves the way for increased understanding of the mechanism of photocurrent generation in carbon nanotubes and/or energy transfer processes from photoactive molecules. This understanding will help to develop future applications of carbon nanotubes in solar cells and light-sensitive devices.

## METHODS

HiPco SWCNT raw material (NanoIntegris) was used throughout this work. In order to prepare suspensions for (*n*, *m*) purification, 20 mg of raw SWCNT material was suspended in 80 mL of $H_2O$ with 2 wt % sodium dodecyl sulfate (SDS) using a tip sonicator (Weber Ultrasonics, 35 kHz, 500 W, in continuous mode) applied for 15 h at ∼20% power. During sonication, the suspension was placed in a water-circulation bath at 15 °C to aid cooling. As described in detail previously,[3] a SECcurity gel permeation chromatography 1260 Infinity system (Agilent Technologies) was then used to separate this raw SWCNT suspension into (*n*, *m*) pure fractions with the use of sequential 0.2 wt % reductions in SDS concentration and a pH gradient of pH 3−4. Seven milliliters of the Sephacryl S-200 gel medium (Amersham Biosciences) was placed into a commercially available water-jacketed liquid chromatography column (XK 16/20, GE Healthcare) with 16 mm inner diameter and 20 cm length. After applying slight compression the gel yielded a final height of 2 cm. An Accel 250 LC water chiller (Thermoscientific) was used to maintain the column temperature at 23 °C. Absorption spectra of the sorted fractions were recorded on a Varian Cary 500 spectrophotometer.

Dielectrophoresis was then used to deposit the prepared (*n*, *m*) SWCNT suspensions into devices for photocurrent measurements. An array of metallic contacts (where each contact constitutes a device) was patterned on a degenerately doped silicon substrate with an 800 nm layer of silicon dioxide using standard electron beam lithography and a PMMA resist. Following lithography 5 nm of titanium and 50 nm of palladium were deposited by sputtering before a final lift-off process was performed in acetone. The resultant metallic contacts had a width of 1 $\mu$m and a gap-size of 600 nm. A 30 $\mu$L amount of diluted SWCNT suspension was then dropped onto the array of metallic contacts, and an alternating voltage was applied to the silicon substrate and one common metallic electrode. In this way, SWCNTs were deposited simultaneously into multiple devices.[13] Typical deposition parameters were frequency $f$ = 1 MHz, peak-to-peak voltage $V_{pp}$ = 6 V, and time $t$ = 15 min. The nanotube suspension was used without dilution and resulted in a CNT density of approximately 10/$\mu$m except for the device shown in Figure 4, where we had approximately 10 times the surface density. Scanning electron microscopy of resultant devices was taken with a Zeiss Ultra Plus.

Photocurrent measurements were taken with a SuperK Extreme EXW-6 broadband supercontinuum light source (NKT Photonics), where the excitation wavelength was tuned between 500 and 825 nm with the use of the SuperK Select acousto-optic tunable filter (NKT Photonics). The resultant light was linearly polarized and had a bandwidth of 5 nm. A microscope objective of numerical aperture 0.5 was then used to focus the quasi-monochromatic light onto an SWCNT device with an intensity of a few hundred microwatts. This corresponds to a diffraction-limited laser spot of diameter less than 1 $\mu$m, which is comparable to the channel length (metallic contact gap-size) of the device. With the help of a motorized $x-y$ stage the fabricated devices were also scanned with a spatial resolution of 375 nm to produce a "photocurrent map". Furthermore, the elastically scattered light was measured with a silicon photodiode and overlaid on the photocurrent map to allow for the position of the photocurrent relative to the SWCNT device to be determined. The resolution is consequently determined by the laser spot diameter and the step size of the motorized stage. The generated zero-bias photocurrent signal was measured with a Keithley 6430 source meter.

*Conflict of Interest:* The authors declare no competing financial interest.

*Acknowledgment.* The authors gratefully acknowledge Martin Pfeiffer for assistance with LabVIEW. B.S.F. gratefully acknowledges support from the Deutsche Forschungsgemeinschaft's Emmy Noether Program under grant number FL 834/1-1.

R.K. acknowledges support by the Deutsche Forschungsgemeinschaft (INTST 163/354-1 FUGG). This research was also supported by the Bundesministerium fur Bildung und Forschung (BMBF) as administered by POF-NanoMicro.

*Supporting Information Available:* Complete absorption spectra of the SWCNT material used in this work and representative transconductance curves are provided. This material is available free of charge *via* the Internet at http://pubs.acs.org.

## REFERENCES AND NOTES


1. Tune, D. D.; Flavel, B. S.; Krupke, R.; Shapter, J. G. Carbon Nanotube-Silicon Solar Cells. *Adv. Energy Mater.* **2012**, *2*, 1043–1055.
2. Flavel, B. S.; Kappes, M. M.; Krupke, R.; Hennrich, F. Separation of Single-Walled Carbon Nanotubes by 1-Dodecanol-Mediated Size-Exclusion Chromatography. *ACS Nano* **2013**, *7*, 3557–3564.
3. Flavel, B. S.; Moore, K. E.; Pfohl, M.; Kappes, M. M.; Hennrich, F. Separation of Single-Walled Carbon Nanotubes with a Gel Permeation Chromatography System. *ACS Nano* **2014**, *8*, 1817–1826.
4. Tune, D. D.; Shapter, J. G. The Potential Sunlight Harvesting Efficiency of Carbon Nanotube Solar Cells. *Energ. Environ. Sci.* **2013**, *6*, 2572–2577.
5. Barone, P. W.; Baik, S.; Heller, D. A.; Strano, M. S. Near-Infrared Optical Sensors Based on Single-Walled Carbon Nanotubes. *Nat. Mater.* **2005**, *4*, 86–U16.
6. Gabor, N. M.; Zhong, Z. H.; Bosnick, K.; Park, J.; McEuen, P. L. Extremely Efficient Multiple Electron-Hole Pair Generation in Carbon Nanotube Photodiodes. *Science* **2009**, *325*, 1367–1371.
7. Svrcek, V.; Cook, S.; Kazaoui, S.; Kondo, M. Silicon Nanocrystals and Semiconducting Single-Walled Carbon Nanotubes Applied to Photovoltaic Cells. *J. Phys. Chem. Lett.* **2011**, *2*, 1646–1650.
8. Bindl, D. J.; Safron, N. S.; Arnold, M. S. Dissociating Excitons Photogenerated in Semiconducting Carbon Nanotubes at Polymeric Photovoltaic Heterojunction Interfaces. *ACS Nano* **2010**, *4*, 5657–5664.
9. Bindl, D. J.; Wu, M. Y.; Prehn, F. C.; Arnold, M. S. Efficiently Harvesting Excitons from Electronic Type-Controlled Semiconducting Carbon Nanotube Films. *Nano Lett.* **2011**, *11*, 455–460.
10. Jain, R. M.; Howden, R.; Tvrdy, K.; Shimizu, S.; Hilmer, A. J.; McNicholas, T. P.; Gleason, K. K.; Strano, M. S. Polymer-Free Near-Infrared Photovoltaics with Single Chirality (6,5) Semiconducting Carbon Nanotube Active Layers. *Adv. Mater.* **2012**, *24*, 4436–4439.
11. Shea, M. J.; Arnold, M. S. 1% Solar Cells Derived from Ultrathin Carbon Nanotube Photoabsorbing Films. *Appl. Phys. Lett.* **2013**, *102*, 243101.
12. Krupke, R.; Hennrich, F.; Weber, H. B.; Beckmann, D.; Hampe, O.; Malik, S.; Kappes, M. M.; Lohneysen, H. V. Contacting Single Bundles of Carbon Nanotubes with Alternating Electric Fields. *Appl. Phys. A: Mater. Sci. Process.* **2003**, *76*, 397–400.
13. Vijayaraghavan, A.; Blatt, S.; Weissenberger, D.; Oron-Carl, M.; Hennrich, F.; Gerthsen, D.; Hahn, H.; Krupke, R. Ultra-Large-Scale Directed Assembly of Single-Walled Carbon Nanotube Devices. *Nano Lett.* **2007**, *7*, 1556–1560.
14. Avouris, P.; Freitag, M.; Perebeinos, V. Carbon-Nanotube Photonics and Optoelectronics. *Nat. Photonics* **2008**, *2*, 341–350.
15. Balasubramanian, K.; Burghard, M.; Kern, K.; Scolari, M.; Mews, A. Photocurrent Imaging of Charge Transport Barriers in Carbon Nanotube Devices. *Nano Lett.* **2005**, *5*, 507–510.
16. Chen, C. X.; Lu, Y.; Kong, E. S.; Zhang, Y. F.; Lee, S. T. Nanowelded Carbon-Nanotube-Based Solar Microcells. *Small* **2008**, *4*, 1313–1318.
17. Engel, M.; Steiner, M.; Sundaram, R. S.; Krupke, R.; Green, A. A.; Hersam, M. C.; Avouris, P. Spatially Resolved Electrostatic Potential and Photocurrent Generation in Carbon Nanotube Array Devices. *ACS Nano* **2012**, *6*, 7303–7310.
18. Freitag, M.; Martin, Y.; Misewich, J. A.; Martel, R.; Avouris, P. H. Photoconductivity of Single Carbon Nanotubes. *Nano Lett.* **2003**, *3*, 1067–1071.
19. Lee, J. U.; Gipp, P. P.; Heller, C. M. Carbon Nanotube p-n Junction Diodes. *Appl. Phys. Lett.* **2004**, *85*, 145–147.
20. Barkelid, M.; Zwiller, V. Single Carbon Nanotube Photovoltaic Device. *J. Appl. Phys.* **2013**, *114*, 154320.
21. Barkelid, M.; Zwiller, V. Photocurrent Generation in Semiconducting and Metallic Carbon Nanotubes. *Nat. Photonics* **2014**, *8*, 48–52.
22. Lee, J. U. Photovoltaic Effect in Ideal Carbon Nanotube Diodes. *Appl. Phys. Lett.* **2005**, *87*, 073101.
23. St-Antoine, B. C.; Menard, D.; Martel, R. Position Sensitive Photothermoelectric Effect in Suspended Single-Walled Carbon Nanotube Films. *Nano Lett.* **2009**, *9*, 3503–3508.
24. Tsen, A. W.; Donev, L. A. K.; Kurt, H.; Herman, L. H.; Park, J. Imaging the Electrical Conductance of Individual Carbon Nanotubes with Photothermal Current Microscopy. *Nat. Nanotechnol.* **2009**, *4*, 108–113.
25. Zhang, Y.; Iijima, S. Elastic Response of Carbon Nanotube Bundles to Visible Light. *Phys. Rev. Lett.* **1999**, *82*, 3472–3475.
26. St-Antoine, B. C.; Menard, D.; Martel, R. Photothermoelectric Effects in Single-Walled Carbon Nanotube Films: Reinterpreting Scanning Photocurrent Experiments. *Nano Res.* **2012**, *5*, 73–81.
27. Sczygelski, E.; Sangwan, V. K.; Wu, C. C.; Arnold, H. N.; Everaerts, K.; Marks, T. J.; Hersam, M. C.; Lauhon, L. J. Extrinsic and Intrinsic Photoresponse in Monodisperse Carbon Nanotube Thin Film Transistors. *Appl. Phys. Lett.* **2013**, 102.
28. Amer, M. R.; Chang, S. W.; Dhall, R.; Qiu, J.; Cronin, S. B. Zener Tunneling and Photocurrent Generation in Quasi-Metallic Carbon Nanotube pn-Devices. *Nano Lett.* **2013**, *13*, 5129–5134.
29. DeBorde, T.; Aspitarte, L.; Sharf, T.; Kevek, J. W.; Minot, E. D. Photothermoelectric Effect in Suspended Semiconducting Carbon Nanotubes. *ACS Nano* **2014**, *8*, 216–221.
30. DeBorde, T.; Aspitarte, L.; Sharf, T.; Kevek, J. W.; Minot, E. D. Determining the Chiral Index of Semiconducting Carbon Nanotubes Using Photoconductivity Resonances. *J. Phys. Chem. C* **2014**, *118*, 9946–9950.
31. Liu, K. H.; Hong, X. P.; Zhou, Q.; Jin, C. H.; Li, J. H.; Zhou, W. W.; Liu, J.; Wang, E. G.; Zettl, A.; Wang, F. High-Throughput Optical Imaging and Spectroscopy of Individual Carbon Nanotubes in Devices. *Nat. Nanotechnol.* **2013**, *8*, 917–922.
32. Tu, X. M.; Manohar, S.; Jagota, A.; Zheng, M. DNA Sequence Motifs for Structure-Specific Recognition and Separation of Carbon Nanotubes. *Nature* **2009**, *460*, 250–253.
33. Arnold, M. S.; Green, A. A.; Hulvat, J. F.; Stupp, S. I.; Hersam, M. C. Sorting Carbon Nanotubes by Electronic Structure Using Density Differentiation. *Nat. Nanotechnol.* **2006**, *1*, 60–65.
34. Arnold, M. S.; Stupp, S. I.; Hersam, M. C. Enrichment of Single-Walled Carbon Nanotubes by Diameter in Density Gradients. *Nano Lett.* **2005**, *5*, 713–718.
35. Ghosh, S.; Bachilo, S. M.; Weisman, R. B. Advanced Sorting of Single-Walled Carbon Nanotubes by Nonlinear Density-Gradient Ultracentrifugation. *Nat. Nanotechnol.* **2010**, *5*, 443–450.
36. Liu, H. P.; Tanaka, T.; Urabe, Y.; Kataura, H. High-Efficiency Single-Chirality Separation of Carbon Nanotubes Using Temperature-Controlled Gel Chromatography. *Nano Lett.* **2013**, *13*, 1996–2003.
37. Moshammer, K.; Hennrich, F.; Kappes, M. M. Selective Suspension in Aqueous Sodium Dodecyl Sulfate According to Electronic Structure Type Allows Simple Separation of Metallic from Semiconducting Single-Walled Carbon Nanotubes. *Nano Res.* **2009**, *2*, 599–606.
38. Tvrdy, K.; Jain, R. M.; Han, R.; Hilmer, A. J.; McNicholas, T. P.; Strano, M. S. A Kinetic Model for the Deterministic Prediction of Gel-Based Single-Chirality Single-Walled Carbon Nanotube Separation. *ACS Nano* **2013**, *7*, 1779–1789.

39. Sfeir, M. Y.; Misewich, J. A.; Rosenblatt, S.; Wu, Y.; Voisin, C.; Yan, H.; Berciaud, S.; Heinz, T. F.; Chandra, B.; Caldwell, R.; *et al*. Infrared Spectra of Individual Semiconducting Single-Walled Carbon Nanotubes: Testing the Scaling of Transition Energies for Large Diameter Nanotubes. *Phys. Rev. B* **2010**, 195424.
40. Mohite, A.; Lin, J.; Sumanasekera, G. U.; Alphenaar, B. W. Field-Enhanced Photocurrent Spectroscopy of Excitonic States in Single-Wall Carbon Nanotubes. *Nano Lett.* **2006**, 1369–1373.
41. Okazaki, T.; Saito, T.; Matsuura, K.; Ohshima, S.; Yumura, M.; Iijima, S. Photoluminescence Mapping of "As-Grown" Single-Walled Carbon Nanotubes: A Comparison with Micelle-Encapsulated Nanotube Solutions. *Nano Lett.* **2005**, *5*, 2618–2623.
42. Lefebvre, J.; Fraser, J. M.; Homma, Y.; Finnie, P. Photoluminescence from Single-Walled Carbon Nanotubes: A Comparison Between Suspended and Micelle-Encapsulated Nanotubes. *Appl. Phys. A: Mater. Sci. Process.* **2004**, *78*, 1107–1110.
43. Choi, J. H.; Strano, M. S. Solvatochromism in Single-Walled Carbon Nanotubes. *Appl. Phys. Lett.* **2007**, *90*, 223114.
44. Fantini, C.; Jorio, A.; Souza, M.; Strano, M. S.; Dresselhaus, M. S.; Pimenta, M. A. Optical Transition Energies for Carbon Nanotubes from Resonant Raman Spectroscopy: Environment and Temperature Effects. *Phys. Rev. Lett.* **2004**, *93*, 147406.
45. Benedict, L. X.; Louie, S. G.; Cohen, M. L. Static Polarizabilities of Single-Wall Carbon Nanotubes. *Phys. Rev. B* **1995**, *52*, 8541–8549.
46. Kozinsky, B.; Marzari, N. Static Dielectric Properties of Carbon Nanotubes from First Principles. *Phys. Rev. Lett.* **2006**, *96*, 166801.